ACS APPLIED MATERIALS & INTERFACES

Research Article

www.acsami.org

Plasmon Resonance Enhanced Optical Absorption in Inverted Polymer/Fullerene Solar Cells with Metal Nanoparticle-Doped Solution-Processable TiO_2 Layer

Mei-Feng Xu, Xiao-Zhao Zhu, Xiao-Bo Shi, Jian Liang, Yue Jin, Zhao-Kui Wang,* and Liang-Sheng Liao*

Jiangsu Key Laboratory for Carbon-Based Functional Materials & Devices, Institute of Functional Nano & Soft Materials (FUNSOM), Soochow University, Suzhou, Jiangsu 215123, China

Supporting Information

ABSTRACT: This paper investigates the effects of localized surface plasmon resonance (LSPR) in an inverted polymer/fullerene solar cell by incorporating Au and/or Ag nanoparticles (NPs) into the TiO_2 buffer layer. Enhanced light harvesting via plasmonic resonance of metal NPs has been observed. It results in improved short-circuit current density (J_{sc}) while the corresponding open-circuit voltage (V_{oc}) is maintained. A maximum power conversion efficiency of 7.52% is obtained in the case of introducing 30% Ag NPs into the TiO_2, corresponding to a 20.7% enhancement compared with the reference device without the metal NPs. The device photovoltaic characteristics, photocurrent properties, steady-state and dynamic photoluminescences of active layer on metal NP-doped TiO_2, and electric field profile in metal NP-doped TiO_2 layers are systematically investigated to explore how the plasmonic effects of Au and/or Ag NPs influence the OSC performance.

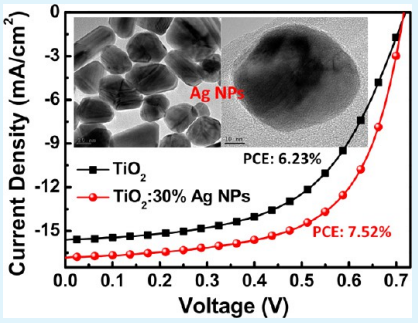

KEYWORDS: *polymer solar cells, metal nanoparticles, localized surface plasmon resonance*

1. INTRODUCTION

Organic solar cells (OSCs) have attracted considerable attention owing to their advantages of lightweight, low cost, mechanical flexibility, and so on.[1−4] In past decades, the cell efficiency has been improved step by step up to 10%.[5] For the favorable competition with fossil fuels, further efforts to increase the power conversion efficiency while lowering the cost and improving the device stability are necessary to realize their industrialization. Recently, OSCs with an inverted structure have drawn great interest owing to the improved cell stability, the flexibility in designing tandem devices, and the compatibility to mass production.[6,7] In addition, a blending film by mixing a conjugated polymer as the donor and a fullerene as the acceptor known as bulk heterojunctions (BHJs) structure can increase the interface area and enlarge the diffusion length of short excitons for higher device performance. It is known that light absorption in OSCs creates strongly bound electron−hole pairs (excitons) which need to diffuse to a donor/acceptor interface to be dissociated into free charges. Whereas, there exists a trade-off between light absorption and exciton harvesting efficiency because of complicated design and optimization of OSC devices. The optical absorption can be enhanced by increasing the thickness of active layer, while thicker films usually cause higher device resistance. Many other strategies, e.g., using folded device architectures, aperiodic dielectric stacks, diffraction gratings and plasmon resonant metallic nanostructures, have been explored to improve light-harvesting efficiency in OSCs.[4] Among them, an effective approach to tackling this issue is the exploration of metal nanoparticles (NPs) with its excited localized surface plasmon resonance (LSPR) effect.[8] The excitation of LSPR through the resonant interaction between the electromagnetic field of incident light and the surface electron density surrounding the NPs causes local enhancement in the electromagnetic field, which is expected to enhance light harvesting in OSCs devices.[9,10]

Efficiency enhancements in OSCs through the introduction of NPs into devices, such as directly patterning on the interfaces of anode and cathode,[11−15] doping into the anode buffer layer poly (3, 4-ethylenedioxythiophene)-polystyrene-sulfonic acid (PEDOT:PSS),[16−18] in tandem OSCs,[19,20] and even in active layers,[21] have been investigated experimentally. However, a comprehensive understanding of the plasmonic effects from metal NPs in OSCs remains inconclusive. In this paper, we demonstrate an inverted polymer/fullerene OSC by doping Au and/or Ag NPs into the cathode buffer layer of TiO_2. Increased short-circuit current density (J_{sc}) with the same open-circuit voltage (V_{oc}) is observed in the devices containing Ag NPs, resulting in a 20.7% enhancement in power conversion efficiency (from 6.23% to 7.52%) compared with the reference device without metal NPs. The effects of Au and/or Ag NPs on the OSC performance are systematically investigated by a combined evaluation of metal NPs size, surface morphologies of TiO_2 buffer layer, photovoltaic characteristics, photocurrent

Received: May 30, 2012
Accepted: March 19, 2013
Published: March 19, 2013

   dx.doi.org/10.1021/am4001979 | ACS Appl. Mater. Interfaces 2013, 5, 2935−2942

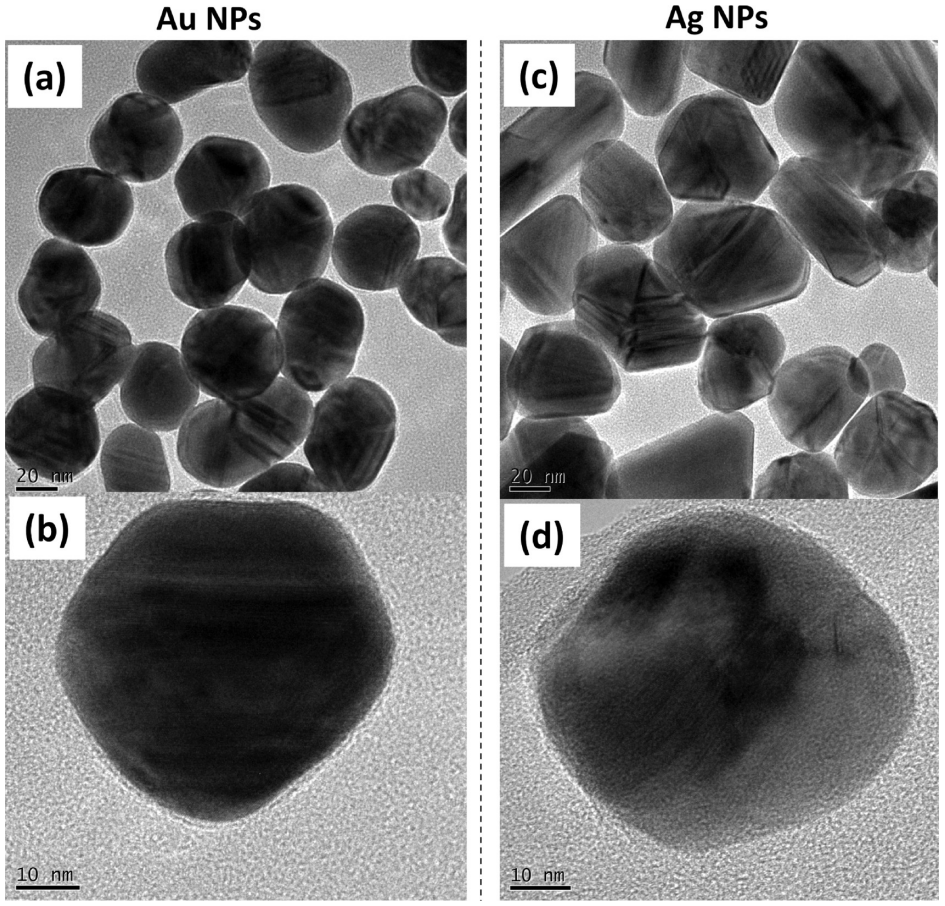

Figure 1. TEM images of (a) Au NPs and (c)Ag NPs; (b, d) same TEM images with high-resolution.

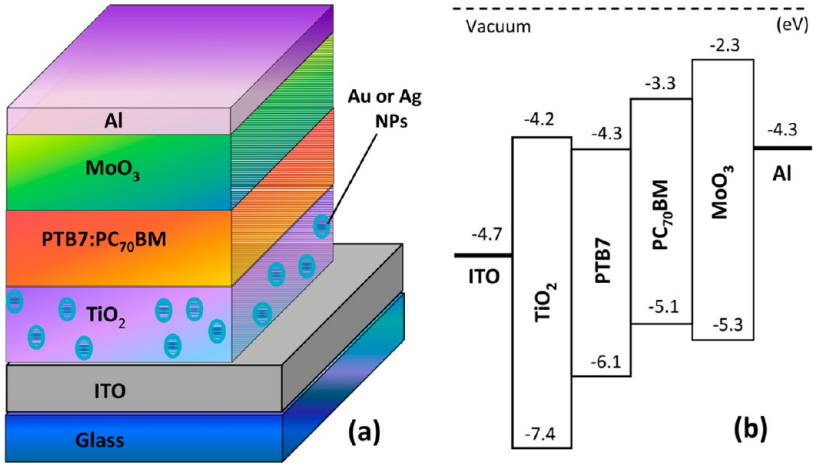

Figure 2. (a) Schematic structure of the photovoltaic device. (b) Energy level diagram of the photovoltaic device.

behavior, steady-state and dynamic photoluminescences, and electric-field profile in Au and/or Ag NP-doped TiO_2 layer by theoretical calculations.

2. EXPERIMENTAL SECTION

The Au NPs and Ag NPs were prepared through the standard sodium citrate reduction method as previously reported.[22,23] The average particle size of the metal NPs were estimated from transmission electron microscopy (TEM) images (FEI Tecnai G^2 F20S-TWIN, at 200 kV). Figure 1 shows the TEM high resolution images of Au NPs and Au NPs. The nanoparticles are spherical in shape and highly dispersed with average diameters of 40 ± 5 nm for Au NPs, and 50 ± 5 nm for Ag NPs.

The TiO_2 film was prepared by a sol−gel method as follows: dissolving of 10 mL tetrabutyl titanate $[Ti(OC_4H_9)_4]$ in 100 mL of ethanol (C_2H_5OH), followed by adding 10 mL of CH_3COOH, then 10 mL of acetylacetone, and 10 mL of deionized water at last. The mixture was stirred at room temperature for 30 min after each reagent was added.[24,25] The prepared metal NPs were then blended into the TiO_2 solution with various volume ratios of 10, 20, 30, and 40%, respectively.

The inverted OSC devices have a configuration of ITO/TiO_2: Ag (or Au) NPs/PTB7:$PC_{70}BM$/MoO_3 (8 nm)/Al (100 nm) as shown in

Figure 2a. The energy levels of the materials used are shown in Figure 2b. The ITO-coated glass substrate was precleaned in subsequent ultrasonic baths of acetone, methanol, and deionized water for 15 min each, followed by an oxygen plasma treatment for 15 min. The TiO_2 film was deposited on ITO by casting the TiO_2 with and without the metal NPs. The samples were then annealed at 400 °C on a hot plate for 2 h. The PTB7:$PC_{70}BM$ blend (PTB7:$PC_{70}BM$ = 1:1.5 by weight) were prepared in chlorobenzene/1,8-diiodoctane (97%:3% by volume) as a concentration of 25 mg/mL, and then, the samples were transferred to the evaporation chamber for evaporating MoO_3 and Al under a pressure of 2×10^{-6} Torr.

The current density−voltage (J−V) characteristics of devices were measured under AM 1.5G (AM = air mass) irradiation with the intensity of 100 mW/cm^2 by a programmable Keithley 2612 source meter. Newport monochromator 74125 and power meter 1918 with silicon detector 918D were used in the incident photontoelectron conversion efficiency (IPCE) measurements. Absorption spectra were recorded by an UV/vis spectrophotometer (PerkinElmer Lambda 750). The topography of the film surface was evaluated by atomic force microscope (AFM) with a Veeco Multimode V instrument. Both the extinction spectra of metal NPs and the absorption spectra of stacked layer TiO_2/PTB7:$PC_{70}BM$ were measured by an UV/vis spectrophotometer (PerkinElmer Lambda 750). Steady state photoluminescence (PL) spectra and transient property were obtained by a Fluorescence spectrometer (Horiba Flworomax-4) and a single photon counting spectrometer which was combined with the Fluorolog-3 spectrofluorometer (Horiba-FM-2015). A 300 nm nano-LED source with pulse duration less than 1 ns was used in the time-resolved PL measurement. The electric-field profiles calculations in the metal NPs-doped TiO_2 layer were also carried out.

3. RESULTS AND DISCUSSION

3.1. Device Photovoltaic Characteristics. First, doping ratio of metal NPs into TiO_2 layer were optimized with the goal of obtaining maximum cell efficiency. In both cases of Au and/or Ag NPs doping, J_{sc} increased gradually with the metal NPs doping ratio from 0 to 30% with almost unaltered V_{oc}. With further increasing of metal NPs doping ratio, e.g., 40%, J_{sc} had a decreased trend, which resulted in deteriorated device efficiency although V_{oc} was still unchangeable. Figure 3 displays the J−V characteristics of devices with and without doping Au and/or Ag NPs (30% concentration) into TiO_2 under illumination of 100 mW/cm^2 (see Figure S1 in the Supporting Information for the other J−V characteristics of the devices with varied doping concentration of the metal NPs). The key cell parameters, including J_{sc}, V_{oc}, fill factor (FF), series resistance (R_s), and power conversion efficiency (PCE) of all devices as a function of Au and/or Ag NPs doping ratio were listed in Table 1. The

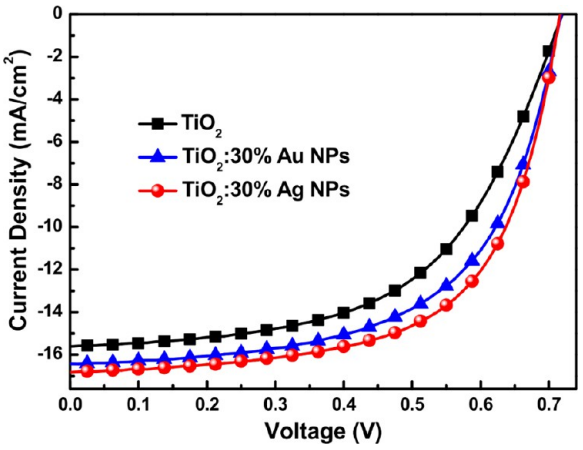

Figure 3. Current density−voltage (J-V) characteristics in the reference device without any metal NPs doping, the device with 30% Au NP-doped TiO_2 layer, and the device with 30% Ag NP-doped TiO_2 layer under 100 mW/cm^2 AM 1.5G simulated solar illuminations.

Table 1. Short-Circuit Current Density (J_{sc}), Open-Circuit Voltage (V_{oc}), Power Conversion Efficiency (PCE), Fill Factor (FF), and Series Resistance (R_s) of Various Inverted PV Devices with Different Buffer Layer

buffer layer	V_{oc} (V)	J_{sc} (mA/cm^2)	FF (%)	PCE (%)	R_s (Ω)
pristine TiO_2	0.71	15.58	56	6.23	113
TiO_2:10% Au NPs	0.70	15.68	61	6.67	48
TiO_2:20% Au NPs	0.71	15.80	61	6.84	40
TiO_2:30% Au NPs	0.71	16.44	60	7.02	38
TiO_2:40% Au NPs	0.70	15.52	59	6.86	52
TiO_2:10% Ag NPs	0.70	15.80	59	6.77	37
TiO_2:20% Ag NPs	0.71	16.50	61	7.15	26
TiO_2:30% Ag NPs	0.71	16.80	63	7.52	25
TiO_2:40% Ag NPs	0.71	16.02	62	7.26	50

reference device (without any metal NPs) had a J_{sc} of 15.58 mA/cm^2, V_{oc} of 0.71 V, FF of 56%, and power conversion efficiency of 6.23%. Upon doping Au NPs into TiO_2, an upward trend in J_{sc} was observed and a maximum power conversion efficiency of 7.02% was achieved with J_{sc} = 16.44 mA/cm^2, V_{oc} = 0.71 V, and FF = 60% in the case of 30% Au NPs doping. Noticeably, V_{oc} remained the same as that of the reference device. The unchangeable V_{oc}, which was different from the decreased V_{oc} in OSCs with introducing a self-assembled layer of metal NPs between the buffer layer and the active layer,[26] suggests that the Au NPs have no large influence on the energy level distribution of the devices. It is widely believed that the V_{oc} mainly originates from the energy difference between the highest occupied molecular orbital (HOMO) of donor and the lowest unoccupied molecular orbital (LUMO) of acceptor.[27] In particular, very similar trend on device parameters occurred in the cases of Ag NPs doping. Nevertheless, a maximum PCE of 7.52% was achieved at 30% Ag NPs doping condition, which was higher than that of Au NP-doped device with the same conditions.

The downward trend of device performance also is supposed to respect with enhanced backward scattering and/or increased resistivity of the buffer layer. As shown in Table 1, the device series resistance was really enlarged from 38 to 52 Ω and 25 to 50 Ω with increased volume ratios of Au and Ag NPs from 30% to 40%, respectively. It suggests that the buffer layers have an effect on the interface morphology near the active layer, which results in larger leakage current, so as to larger series resistance. Figure 4**a**-4**c** shows the typical AFM morphology image of pristine TiO_2, 30% Au NP-doped TiO_2, and 30% Ag NPs-doped TiO_2, respectively. The root-mean-square (rms) roughness of three films was found to be 1.53 nm, 1.80 nm, and 1.61 nm, respectively. This also supports our hypothesis that smooth surface morphology results in good interface contact and improved device performance owing to the avoidance of large leakage current. Figure 5 shows the J−V characteristics of devices incorporating TiO_2 with and without 30% Au and/or Ag NPs under illumination and in dark conditions. After Au and/or Ag NPs were introduced, the reverse dark currents were slightly lowered compared with that in the reference device. In general, the reverse dark current is in respect of the microscopic

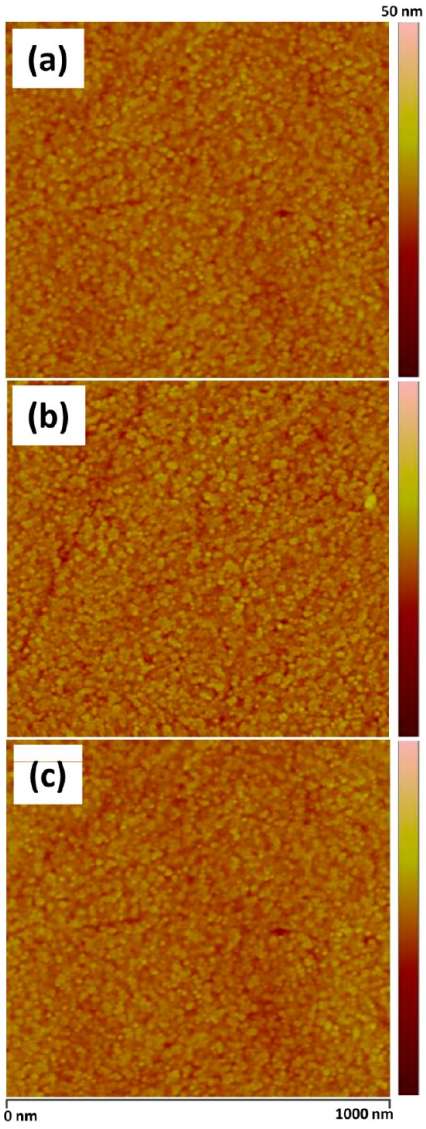

Figure 4. AFM morphology image of (a) pristine TiO_2, (b) 30% Au NP-doped TiO_2, and (c) 30% Ag NP-doped TiO_2.

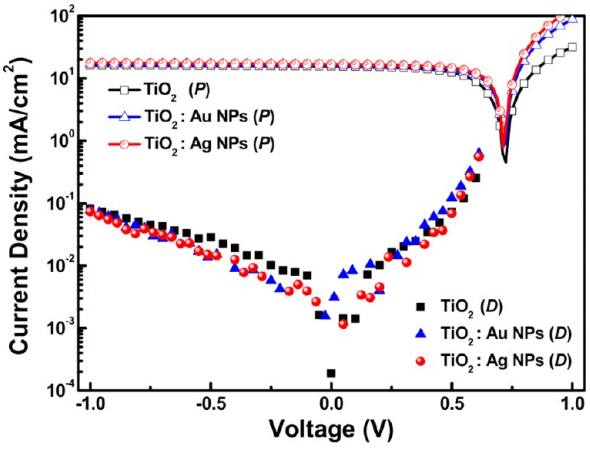

Figure 5. Current density−voltage (J−V) characteristics in the reference device without any metal NPs doping, the device with 30% Au NPs doped TiO_2 layer, and the device with 30% Ag NP-doped TiO_2 layer under 100 mW/cm^2 AM 1.5G simulated solar illuminations and dark conditions.

leak circuit in the device, which usually originates from the bad interfacial contact near the active layer.[28] The reverse dark current evaluations were consistent with the results of device series resistance and the interface morphology measured by AFM.

Figure 6a presents incident photon-to-electron conversion efficiency (IPCE) curves in the devices with and without Au

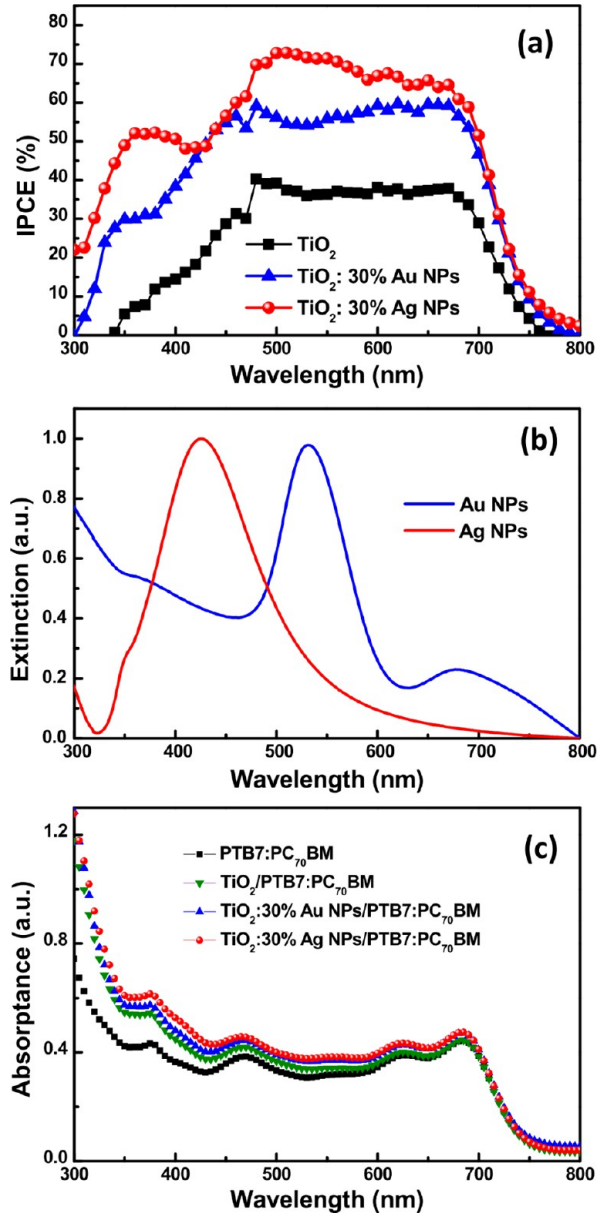

Figure 6. (a) Incident photon-to-electron conversion efficiency (IPCE) curves in the reference device without any metal NPs doping, the device with 30% Au NPs doped TiO_2 layer, and the device with 30% Ag NP-doped TiO_2 layer. (b) Extinction sepctra of Au NPs and Ag NPs solutions. (c) Absorptance spectra of the stacked films of TiO_2/ PTB7:PC_{70}BM, and TiO_2: Au (or Ag) NPs/PTB7:PC_{70}BM.

and/or Ag NPs doping (30% concentration). The photocurrent within the wavelength range from 350 to 700 nm increased significantly after incorporating Au NPs especially Ag NPs into TiO_2.[29,30] In particular, the enhancement peaks at 370 and 510 nm appeared in IPCE curves of metal NPs doped devices. The extinction spectra of Au NPs and Ag NPs solution were also

shown in Figure 6b. The extinction peaks at 530 nm for Au NPs and 420 nm for Ag NPs are within the wavelength regime of the photocurrent generation in both cases of the metal NPs doping. In addition, slight enhancements in stacked films of TiO_2: Au (or Ag) NPs/PTB7:$PC_{70}BM$ in the same wavelength range were also observed compared with the films of TiO_2/PTB7:$PC_{70}BM$ (Figure 6c). We attribute it to the wide absorption range of the metal NPs, and the enhanced LSPR excitation that results in improved device performance. It is associated with the fact of NPs resonance peak depending strongly on the surrounding media.[20,31,32] In general, high optical field intensity in the active layer results in high optical absorption. Therefore, the enhanced absorption is expected to lead to a larger number of photogenerated excitons, and thus a larger photocurrent. In the case of suitable ratio of Ag NPs doping into TiO_2, more excitions can be generated and more holes and electrons would be extracted to respective electrode before their recombination. Consequently, the photocurrent is improved and higher device performance is obtained. When further increasing the NPs concentration, J_{sc} decreased, as shown in Figure S1 in the Supporting Information, these results suggest the increased bimolecular recombination of photogenerated charge carriers on the surface of the NPs and the transformation of incident light to thermal loss by the intrinsic absorption of NPs (i.e., the nonradiative damping of the surface plasmon).[33]

3.2. Photocurrent Evaluations. To further understand the mechanism responsible for the enhanced performance in metal NPs in particular Ag NPs-doped devices, we investigated the exciton dissociation probabilities in devices with pristine TiO_2, 30% Au NPs-doped TiO_2, and 30% Ag NPs-doped TiO_2 as the buffer layer. Figure 7a shows the effect of the LSPR on the photocurrent density (J_{ph}) in three devices. J_{ph} is determined by the equation $J_{ph} = J_L - J_D$. Where, J_L and J_D is the current density measured under illumination and in dark condition respectively. The plot of J_{ph} with respect to the effective voltage ($V_0 - V$), where V_0 is the compensation voltage (defined by the voltage at which the $J_{ph} = 0$)[34−37] and V is the applied voltage, demonstrates two regions. In lower voltage (<0.3 V), the photocurrents in three devices increase sharply with effective voltage. In higher effective voltage, the J_{ph} reached gradually a saturated value. From Figure 7a, with increasing effective voltage, the saturation photocurrent (J_{sat}) in the device with 30% Ag NPs-doped TiO_2 was reached earlier than those in both the device with pristine TiO_2 and the device with 30% Au NPs-doped TiO_2. In general, the saturated photocurrent correlated to the maximum exciton generation rate (G_{max}), which is mainly governed by the light absorption.[35,37] Therefore, the improved J_{ph} suggests that the introduced metal NPs enhance light harvesting in the device. In addition, the exciton dissociation probability at any effective voltage can be obtained directly from the experimental data by comparing the J_{ph} with the experimentally decided J_{sat}. Figure 7b plotted the normalized photocurrent (J_{ph}/J_{sat}) in three devices. The exciton dissociation probability under the short-circuit condition increased from 81.7% to 86.5% after incorporating 30% Ag NPs in TiO_2. Noticeably, the slope of log J_{ph} vs log ($V_0 - V$) in the reference device was steeper than that of the devices with 30% metal NPs. It means that the exciton dissociation probability at high applied voltage, i.e., the maximum power output bias, is largely improved after introducing metal in particular Ag NPs in the TiO_2. An increase in the exciton dissociation probability reduces the recombination rate and, therefore, improves the device performance.

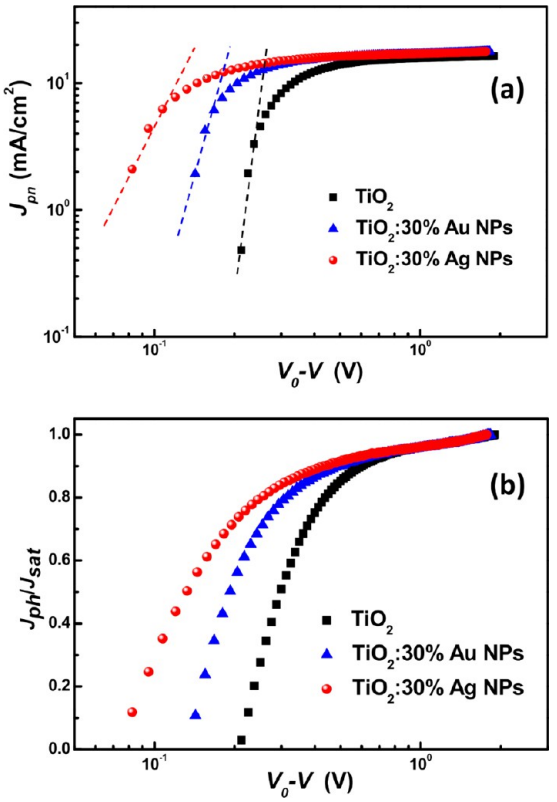

Figure 7. (a) Plots of photocurrent density (J_{ph}) with respect to the effective bias (V_0−V) in the reference device without any metal NPs doping, the device with 30% Au NP-doped TiO_2 layer, and the device with 30% Ag NP-doped TiO_2 layer. (b) Corresponding plots of J_{ph}/J_{sat} with respect to the effective bias (V_0-V) in three devices.

3.3. Plasmonic Effects of Au and/or Ag NPs. To investigate the LSPR effects of Au and/or Ag NPs, the theoretical analog calculations of electric field profiles in metal NPs doped TiO_2 layers were carried out in the wavelength of 370 and 510 nm which corresponds to the peaks in IPCE enhancements in Figure 6a. Figure 8 shows the calculated electric-field profiles in Au NPs and Ag NP-doped TiO_2 layers. The magnitude of the enhanced electric field intensity was indicated by the color scale. It is found that LSPR effects of Au and/or Ag NPs in TiO_2 were excited. Electric field intensity was futherly enhanced in the case of Ag NPs doping. The strong near field caused by LSPR effects from NPs contributed to the improvement of J_{sc}. It suggests that Au and/or Ag NPs can act as an effective "antenna" for the incident sunlight that stores the incident energy in a localized surface plasmon mode.[38]

Steady-state photoluminescence (PL) measurements were further carried out to explore the LSPR effect of Au and/or Ag NPs on the photcurrent behavior. Figure 9 showed the PL spectra of PTB7:$PC_{70}BM$ film on TiO_2 with and without Au and/or Ag NPs doping (30% concentration). The PL spectra showed increasing intensities at about 780 nm upon doping Au and/or Ag NPs. In general, a fluorescence process is associated with the light excitation rate and the quantum yield, which is dependent on the competition between the radiative and nonradiative decay.[16,39] The resonance frequencies of Au NPs and Ag NPs was within the absorption regime of PTB7:$PC_{70}BM$. Therefore, we attributed the enhanced PL

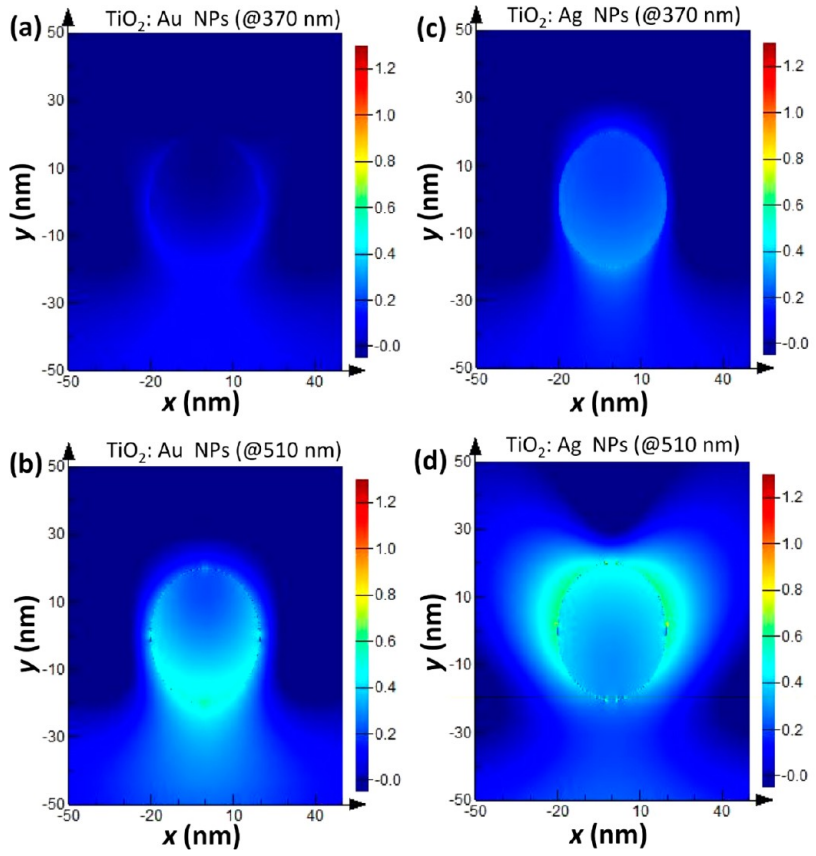

Figure 8. Calculated electric-field profiles in Au NP- and Ag NP-doped TiO_2 layers at wavelengths of 370 and 510 nm. The magnitude of the enhanced electric-field intensity is indicated by the color scale.

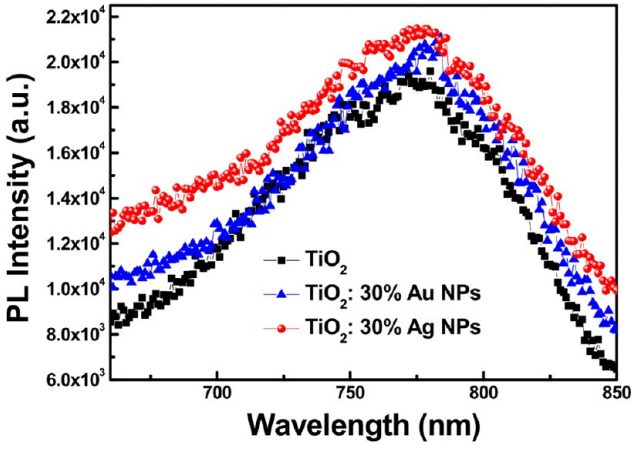

Figure 9. Photoluminescence (PL) spectra of films PTB7:PC_{70}BM, and TiO_2: Au (or Ag) NPs/PTB7:PC_{70}BM.

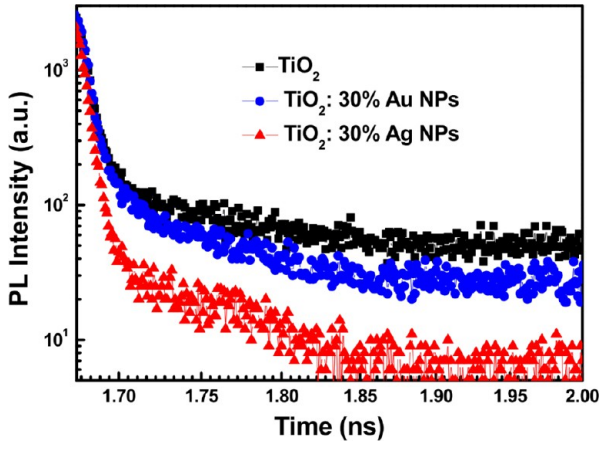

Figure 10. Photoluminescence (PL) decay profiles of films PTB7:PC_{70}BM, and TiO_2: Au (or Ag) NPs/PTB7:PC_{70}BM. A 300 nm nano-LED source with pulse duration less than 1 ns is used for the time-resolved PL measurement.

intensities to the fact that LSPR excitation increased the light absorption, thus enhanced the light excitation rate. It was consistent with our experimental results of exciton dissociation probability evaluation in Figure 7b. In addition, exciton lifetime meansurements by time-resolved PL spectroscopy are very useful for us to probe how the plasmonic effects influence the photocurrent processes in the active layer.[16,40,41] Figure 10 presented the PL intensity decay profiles of PTB7:PC_{70}BM film on TiO_2 with and without Au and/or Ag NPs doping (30% concentration). Obviously, the exciton lifetime was lowered after incorporating Au and/or Ag NPs into TiO_2, which was also attributed to the presence of strong coupling between the plasmonic field and excitons.[9,42] It assumes that the resulting plasmon-exciton coupling participated in the charge transfer process, thus facilitated the exciton dissociation. In addition, the "hot excitons" with excess energy could also overcome their initial Coulombic potential. It means that the generation of hot excitons is beneficial for enhancing the probability of being dissociated into free polarons.[16] As a result, the lifetime of exciton decreased because of the enhanced exciton dissociation through radiative and/or nonradiative processes.[16,39,43,44]

4. CONCLUSION

In summary, we have investigated the effects of Au and/or Ag NPs doped into the TiO_2 buffer layer on the performance of inverted BHJ OSCs based on PTB7:$PC_{70}BM$ blending. Increasing J_{sc} and unchangeable V_{oc} were observed in the devices containing the metal NPs with optimized doping concentration. And a maximum 20.7% enhancement in power conversion efficiency (from 6.23% to 7.52%) was achieved compared with the reference device without metal NPs. The evaluations of device photovoltaic characteristics and photocurrent properties demonstrated that the generation rate and the dissociation probability of excitons were improved after introducing metal NPs, resulting in improved short-circuit current density. By combinating with the measurements of steady state and dynamic photoluminescences of the active layer on the metal NPs doped TiO_2, and electric field profile in the metal NPs doped TiO_2 layers, we found that the improved device performance would be mainly originated from the unique optical properties of the LSPR effects induced by the Au and/or Ag NPs, which leads to an obvious enhancement of light harvesting, and therefore, the improved photocurrent. The solution-processable method provides an alternative for realization of low-cost and flexible OSCs on plastic substrates.

■ ASSOCIATED CONTENT

Supporting Information

The $J-V$ characteristics of reference device without metal NPs doping, the devices with Au NPs doping (varied concentration from 10% to 40%) into TiO_2, and the devices with Ag NPs doping (varied concentration from 10% to 40%) into TiO_2 under illumination of 100 mW/cm^2. The calculated electric field profiles in Au and/or Ag NPs doped TiO_2 layers in different wavelength. These materials are available free of charge via the Internet at http://pubs.acs.org/.

■ AUTHOR INFORMATION

Corresponding Author

*E-mail: lsliao@suda.edu.cn (L.-S.L.); zkwang@suda.edu.cn (Z.-K.W.).

Notes

The authors declare no competing financial interest.

■ ACKNOWLEDGMENTS

We acknowledge financial support from the Natural Science Foundation of China (61036009, 61177016, and 21161160446), the National High-Tech Research Development Program (2011AA03A110), the Natural Science Foundation of Jiangsu Province (BK2010003). This is also a project funded by the Priority Academic Program Development of Jiangsu Higher Education Institutions (PAPD).

■ REFERENCES

(1) Li, G.; Shrotriya, V.; Huang, J.; Yao, Y.; Moriarty, T.; Emery, K.; Yang, Y. *Nat. Mater.* **2005**, *4*, 864−868.
(2) Dennler, G.; Scharber, M. C.; Brabec, C. J. *Adv. Mater.* **2009**, *21*, 1323−1338.
(3) Blom, P. W. M.; Mihailetchi, V. D.; Koster, L. J. A.; Markov, D. E. *Adv. Mater.* **2007**, *19*, 1551−1566.
(4) Wong, W. Y.; Wang, X. Z.; He, Z.; Djurisic, A. B.; Yip, C. T.; Cheung, K. Y.; Wang, H.; Mak, C. S. K.; Chan, W. K. *Nat. Mater.* **2007**, *6*, 521−527.
(5) Green, M. A.; Emery, K.; Hishikawa, Y.; Warta, W.; Dunlop, E. D. *Prog. Photovolt. Res. Appl.* **2012**, *20*, 12−20.
(6) Kuwabara, T.; Kawahara, Y.; Yamaguchi, T.; Takahashi, K. *ACS Appl. Mater. Interfaces* **2009**, *1*, 2107−2110.
(7) Steim, R.; Choulis, S. A.; Schilinsky, P.; Brabec, C. J. *Appl. Phys. Lett.* **2008**, *92*, 093303.
(8) Morfa, A. J.; Rowlen, K. L.; Reilly, T. H., III; Romero, M. J.; Lagemaat, J. v. d. *Appl. Phys. Lett.* **2008**, *92*, 013504.
(9) Lee, J. H.; Park, J. H.; Kim, J. S.; Lee, D. Y.; Cho, K. *Org. Electron.* **2009**, *10*, 416−420.
(10) Reilly, T. H., III; Lagemaat, J. v. d.; Tenent, R. C.; Morfa, A. J.; Rowlen, K. L. *Appl. Phys. Lett.* **2008**, *92*, 243304.
(11) Yakimov, A.; Forrest, S. R. *Appl. Phys. Lett.* **2002**, *80*, 1667.
(12) Kim, S. S.; Na, S. I.; Jo, J.; Kim, D. Y.; Nah, Y. C. *Appl. Phys. Lett.* **2008**, *93*, 073307.
(13) Chen, X.; Zhao, C.; Rothberg, L.; Ng, M. K. *Appl. Phys. Lett.* **2008**, *93*, 123302.
(14) Tsai, S. J.; Ballarotto, M.; Romero, D. B.; Herman, W. N.; Kan, H. C.; Phaneuf, R. J. *Opt. Express* **2010**, *18*, A528−A535.
(15) Kalfagiannis, N.; Karagiannidis, P. G.; Pitsalidis, C.; Panagiotopoulos, N. T.; Gravalidis, C.; Kassavetis, S.; Patsalas, P.; Logothetidis, S. *Sol. Energy Mater. Sol. Cells* **2012**, *104*, 165−174.
(16) Wu, J. L.; Chen, F. C.; Hsiao, Y. S.; Chien, F. C.; Chen, P.; Kuo, C. H.; Huang, M. H.; Hsu, C. S. *ACS Nano* **2011**, *5*, 959−967.
(17) Fung, D. D. S.; Qiao, L.; Choy, W. C. H.; Wang, C.; Sha, W. E. I.; Xie, F.; He, S. *J. Mater. Chem.* **2011**, *21*, 16349−16356.
(18) Qiao, L.; Wang, D.; Zuo, L.; Ye, Y.; Qian, J.; Chen, H.; He, S. *Appl. Energy* **2011**, *88*, 848−852.
(19) Rand, B. P.; Peumans, P.; Forrest, S. R. *J. Appl. Phys.* **2004**, *96*, 7519−7526.
(20) Pan, S.; Rothberg, L. J. *Proc. SPIE* **2007**, *6641*, 736011.
(21) Takeuchi, N.; Kanai, Y.; Selloni, A. *J. Phys. Chem. C* **2010**, *114*, 3981−3986.
(22) Enstn, B.; Turkevich, J. *J. Am. Chem. Soc.* **1963**, *85*, 3317−3328.
(23) Sun, Y.; Xia, Y. *Science* **2002**, *298*, 2176−2179.
(24) Shen, L.; Zhu, G.; Guo, W.; Tao, C.; Zhang, X.; Liu, C.; Chen, W.; Ruan, S.; Zhong, Z. *Appl. Phys. Lett.* **2008**, *92*, 073307.
(25) Kong, X.; Liu, C.; Dong, W.; Zhang, X.; Tao, C.; Shen, L.; Zhou, J.; Fei, Y.; Ruan, S. *Appl. Phys. Lett.* **2009**, *94*, 123502.
(26) Yoon, W. J.; Jung, K. Y.; Liu, J.; Duraisamy, T.; Revur, R.; Teixeira, F. L.; Sengupta, S.; Berger, P. R. *Sol. Energy Mater. Sol. Cells* **2010**, *94*, 128−132.
(27) Lo, M. F.; Ng, T. W.; Liu, T. Z.; Roy, V. A. L.; Lai, S. L.; Fung, M. K.; Lee, C. S.; Lee, S. T. *Appl. Phys. Lett.* **2010**, *96*, 113303.
(28) Lou, Y.; Wang, Z.; Naka, S.; Okada, H. *Appl. Phys. Lett.* **2011**, *99*, 033305.
(29) Brown, K. R.; Natan, M. J. *Langmuir* **1998**, *14*, 726−728.
(30) Talley, C. E.; Jackson, J. B.; Oubre, C.; Grady, N. K.; Hollars, C. W.; Lane, S. M.; Huser, T. R.; Nordlander, P.; Halas, N. J. *Nano lett.* **2005**, *5*, 1569−1574.
(31) Kelly, K. L.; Coronado, E.; Zhao, L. L.; Schatz, G. C. *J. Phys. Chem. B* **2002**, *107*, 668−677.
(32) Pelton, M.; Aizpurua, J.; Bryant, G. *Laser Photonics Rev.* **2008**, *2*, 136−139.
(33) Noh, H. S.; Cho, E. H.; Kim, H. M.; Han, Y. D.; Joo, J. *Org. Electron.* **2012**, *14*, 278−285.
(34) Mihailetchi, V. D.; Xie, H. X.; de Boer, B.; Koster, L. J. A.; Blom, P. W. M. *Adv. Funct. Mater.* **2006**, *16*, 699−708.
(35) Shrotriya, V.; Yao, Y.; Li, G.; Yang, Y. *Appl. Phys. Lett.* **2006**, *89*, 063505.
(36) Mandoc, M. M.; Veurman, W.; Koster, L. J. A.; de Boer, B.; Blom, P. W. M. *Adv. Funct. Mater.* **2007**, *17*, 2167−2173.
(37) Chen, F. C.; Wu, J. L.; Lee, C. L.; Hong, Y.; Kuo, C. H.; Huang, M. H. *Appl. Phys. Lett.* **2009**, *95*, 013305.
(38) Atwater, H. A.; Polman, A. *Nat. Mater.* **2010**, *9*, 205−213.
(39) Anger, P.; Bharadwaj, P.; Novotny, L. *Phys. Rev. Lett.* **2006**, *96*, 113002.
(40) Huang, J. H.; Yang, C. Y.; Ho, Z. Y.; Kekuda, D.; Wu, M. C.; Chien, F. C.; Chen, P.; Chu, C. W.; Ho, K. C. *Org. Electron.* **2009**, *10*, 27−33.

(41) Huang, J. H.; Li, K. C.; Chien, F. C.; Hsiao, Y. S.; Kekuda, D.; Chen, P.; Lin, H. C.; Ho, K. C.; Chu, C. W. *J. Phys. Chem. C* **2010**, *114*, 9062−9069.
(42) Ohkita, H.; Cook, S.; Astuti, Y.; Duffy, W.; Tierney, S.; Zhang, W.; Heeney, M.; McCulloch, I.; Nelson, J.; Bradley, D. D. C.; Durrant, J. R. *J. Am. Chem. Soc.* **2008**, *130*, 3030−3042.
(43) Moet, D. J. D.; Lenes, M.; Morana, M.; Azimi, H.; Brabec, C. J.; Blom, P. W. M. *Appl. Phys. Lett.* **2010**, *96*, 213506.
(44) Mandoc, M. M.; Veurman, W.; Koster, L. J. A.; de Boer, B.; Blom, P. W. M. *Adv. Funct. Mater.* **2007**, *17*, 2167−2173.